

DAMamba: Vision State Space Model with Dynamic Adaptive Scan

Tanzhe Li^{1,2*} Caoshuo Li^{1,2*} Jiayi Lyu³ Hongjuan Pei³ Baochang Zhang⁴ Taisong Jin^{1,2†} Rongrong Ji^{1,2}

Abstract

State space models (SSMs) have recently garnered significant attention in computer vision. However, due to the unique characteristics of image data, adapting SSMs from natural language processing to computer vision has not outperformed the state-of-the-art convolutional neural networks (CNNs) and Vision Transformers (ViTs). Existing vision SSMs primarily leverage manually designed scans to flatten image patches into sequences locally or globally. This approach disrupts the original semantic spatial adjacency of the image and lacks flexibility, making it difficult to capture complex image structures. To address this limitation, we propose Dynamic Adaptive Scan (DAS), a data-driven method that adaptively allocates scanning orders and regions. This enables more flexible modeling capabilities while maintaining linear computational complexity and global modeling capacity. Based on DAS, we further propose the vision backbone DAMamba, which significantly outperforms current state-of-the-art vision Mamba models in vision tasks such as image classification, object detection, instance segmentation, and semantic segmentation. Notably, it surpasses some of the latest state-of-the-art CNNs and ViTs. Code will be available at <https://github.com/ltzovo/DAMamba>.

1. Introduction

In recent years, to tackle the limitations of traditional convolutional neural networks (CNNs) (LeCun et al., 1998) in modeling long-range dependencies, Transformer (Vaswani

*Equal contribution †Corresponding author ¹Key Laboratory of Multimedia Trusted Perception and Efficient Computing, Ministry of Education of China, Xiamen University, China. ²School of Informatics, Xiamen University, China. ³School of Engineering Science, University of Chinese Academy of Sciences, China. ⁴School of Artificial Intelligence, Beihang University, China. Correspondence to: Taisong Jin <jintaisong@xmu.edu.cn>.

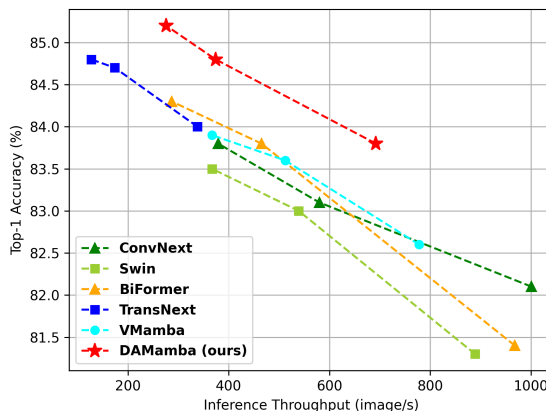


Figure 1. The trade-off between ImageNet-1K top-1 accuracy and inference throughput. All the models are trained under the DeiT training hyperparameters. The inference throughput is measured on an NVIDIA RTX 3090 GPU with a batch size 128. It can be seen that under the same inference throughput or accuracy, the accuracy or inference throughput of the proposed DAMamba significantly outperforms the SSMs, ViTs and CNNs, indicating that the proposed DAMamba achieves **state-of-the-art performance and efficiency**.

et al., 2017) have been introduced into computer vision, achieving state-of-the-art performance in image classification task. However, the self-attention mechanism within Transformer, due to its quadratic computational complexity, faces limitations when applied to high-resolution vision downstream tasks such as object detection and image segmentation. To address this issue, researchers have proposed various sparse attention mechanisms (Wang et al., 2021; 2022; Xia et al., 2022; Dong et al., 2022; Zhu et al., 2023; Jiao et al., 2023; Zhang et al., 2024; Shi, 2024). These mechanisms reduce complexity by introducing sparsity into attention computations, but this usually comes at the expense of the model’s global modeling capability, limiting their performance in real applications.

State space models (SSMs) (Gu et al., 2021), represented by Mamba (Gu & Dao, 2023), have recently garnered significant attention from researchers. The core module, the S6 block, selectively retains or discards information based on the relevance of each element in a sequence. By incor-

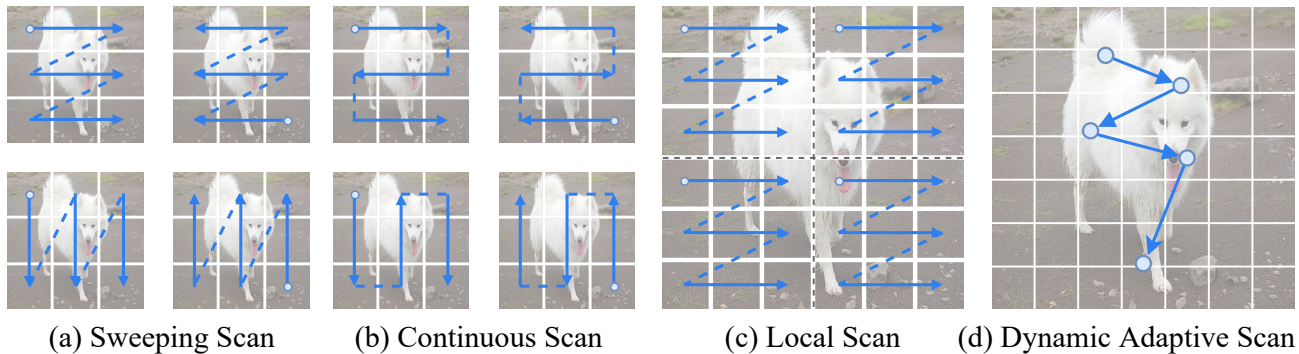


Figure 2. Illustration of different scanning methods in vision state space models. As showed in Figure (a), (b), and (c): previous methods such as Vim (Zhu et al., 2024), VMamba (Liu et al., 2024), PlainMamba (Yang et al., 2024), and LocalMamba (Huang et al., 2024) relies on manually designed global or local scanning methods. These fixed processing approaches lack flexibility and struggle to capture complex image structures. In the Figure (d), we propose a novel scanning method that adaptively allocates scanning order and regions through a data-driven approach. This not only achieves more flexible modeling capabilities but also maintains Mamba’s linear computational complexity and global modeling capacity.

porating a selective mechanism for parallel computation alongside hardware-aware optimization, the S6 block not only offers a comprehensive global receptive field but also attains a computational complexity that scales linearly with the sequence length. This characteristic enables Mamba to outperform popular Transformer models in natural language processing tasks. Inspired by Mamba, some research efforts, such as Vim (Zhu et al., 2024) and VMamba (Liu et al., 2024), have extended its application to computer vision. These approaches divide 2D images into patches and adopt specific scanning strategies to flatten the images into multiple 1D sequences from different directions. This successfully integrates the Mamba model into vision tasks, achieving promising performance and showcasing the potential of SSMs in computer vision.

Unlike one-dimensional sequential language data, visual data typically exhibits two-dimensional spatial structure. One of the core challenges in adapting the Mamba model for vision tasks lies in designing an appropriate scanning strategy for an image. Scanning strategy enables SSMs, which are designed for 1D sequence processing, to effectively accommodate the 2D spatial structure of images. Currently, scanning strategies for vision SSMs can be broadly categorized into three types: sweeping scan, continuous scan, and local scan. Vim and VMamba adopt the sweeping scan strategy, simulating a row-by-row scan from left to right and top to bottom, allowing Mamba to adapt to the 2D spatial structure of images. However, PlainMamba (Yang et al., 2024) argues that sweeping scan overlooks the importance of spatial continuity within images and thus introduces the continuous scan strategy to ensure the correlation between adjacent patches. Meanwhile, LocalMamba (Huang et al., 2024) proposes the local scan strategy, aiming to capture the local spatial relationships within images.

Although the aforementioned methods have proven effective in practice, they rely on manually designed scanning patterns that are independent of the input data, which may not be optimal. For instance, sweeping and continuous scan can cause spatially close patches to become distant in SSM computations, resulting in a loss of local information. On the other hand, local scan can capture local spatial relationships, limiting the model’s ability to capture long-range dependencies. Clearly, there is a need for a more flexible scanning strategy that can dynamically adjust the scanning regions based on the characteristics of each input data instance. For example, in the case of an image of a dog, an ideal scan strategy should adaptively focus on the dog’s body while filtering out irrelevant background information. However, such dynamic adjustment is beyond the capabilities of existing manually designed scanning approaches.

To address the aforementioned issues, we propose a flexible and efficient scanning strategy, named Dynamic Adaptive Scan (DAS). Unlike traditional manually designed scanning methods, DAS dynamically learns and adjusts scanning regions and their sequences during training, enabling smarter and more precise feature extraction. Specifically, DAS starts by defining a set of learnable positions, with initial values corresponding to the original locations of each patch. Then, through a learnable offset prediction network (OPN), a set of offset values is generated for each patch. By combining these offset values with the original patch positions, the predicted patch positions are computed. Using bilinear interpolation, these predicted positions are gradient-linked to the feature map, allowing the offsets to be adaptively optimized during training. The predicted patches are arranged from top to bottom and left to right based on their original positions, dynamically forming a new sequence order according to the input data. Through this mechanism, DAS focuses on more

critical regions, capturing important features and complex spatial structures with greater flexibility.

Based on the proposed DAS, we develop a powerful vision Mamba model, termed DAMamba. DAMamba can serve as a versatile vision backbone for various vision tasks. For instance, our DAMamba-T achieves an image classification accuracy of 83.8%, 48.5 AP^b in object detection, 43.4 AP^m in instance segmentation, and 50.3 mIoU in semantic segmentation. These results surpass the previous state-of-the-art Vision Mamba, VMamba, by 1.2% in classification accuracy, 1.2 AP^b, 0.7 AP^m, and 2.3 mIoU. Moreover, DAMamba also outperforms some recent state-of-the-art ViTs and CNNs in these vision tasks, demonstrating its superior performance and various applicability.

2. Related Work

2.1. Vision State Space Models

Although the Transformer (Vaswani et al., 2017) has achieved remarkable success in natural language processing, its quadratic complexity poses challenges when handling long sequence structures. To address this issue, state-space models (Gu et al., 2021) (SSMs), represented by Mamba (Gu & Dao, 2023), have gradually emerged as an alternative to Transformers. In visual tasks, the quadratic complexity of the standard self-attention mechanism similarly presents challenges for processing high-resolution images. Thus, the Vim (Zhu et al., 2024) and VMamba (Liu et al., 2024) attempt to incorporate Mamba into computer vision tasks. However, inputting images into SSM models remains a critical challenge. Vim and VMamba address this by employing bidirectional and four-directional scanning strategies to transform image patches into one-dimensional sequences. Building on this, subsequent research introduced continuous scanning (Yang et al., 2024) and local four-directional scan (Huang et al., 2024) to better align with the two-dimensional structure of images. Despite the significant achievements of Mamba models in computer vision, existing scanning methods heavily rely on manual design, making it difficult to dynamically and flexibly adapt to input variations. This limitation hinders the model’s ability to capture complex two-dimensional structures. Therefore, our goal is to propose a vision Mamba model capable of adaptively and flexibly adjusting scanning paths based on input image, further enhancing its performance in vision tasks.

2.2. Vision Transformers

The Transformer (Vaswani et al., 2017) model was first introduced in 2017 for natural language processing (NLP) tasks. With its powerful global modeling capabilities and excellent parallelism, the Transformer quickly gained pop-

ularity in the NLP. By the end of 2020, Vision Transformer (Dosovitskiy et al., 2021) (ViT) successfully extended the Transformer model to large-scale image classification tasks, achieving state-of-the-art performance. Subsequently, DeiT (Touvron et al., 2021) improved ViT by introducing knowledge distillation (Hinton et al., 2015) and more efficient training strategies, enabling effective training even on relatively small datasets such as ImageNet-1K (Russakovsky et al., 2015). Following this development trajectory, researchers proposed numerous hierarchical Transformer models that reduce computational complexity for high-resolution images through various sparse attention mechanisms. Notable examples include the Swin Transformer (Liu et al., 2021) and PVT (Wang et al., 2021; 2022). Subsequent research (Wang et al., 2021; 2022; Xia et al., 2022; Dong et al., 2022; Zhu et al., 2023; Jiao et al., 2023; Zhang et al., 2024; Shi, 2024) introduced various sparse attention mechanisms to strike a balance between global modeling capability and computational complexity. However, the global modeling capabilities of these improved sparse attention mechanisms still fall short of the standard self-attention mechanism.

2.3. Convolutional Neural Networks

Convolutional Neural Network (CNN) (LeCun et al., 1998) was initially proposed for handwritten digit recognition, but it wasn’t until the introduction of AlexNet (Krizhevsky et al., 2012) in 2012, which triggered the “ImageNet moment,” that the full potential of CNNs was realized. This breakthrough led to a rapid development in computer vision, driven by the resurgence of neural networks, with CNNs becoming the standard architecture for computer vision tasks. During this period, many representative CNN models emerged, such as VGG (Simonyan & Zisserman, 2014), GoogLeNet (Szegedy et al., 2015), ResNet (He et al., 2016), DenseNet (Huang et al., 2017), DCN (Zhang et al., 2019; Wang et al., 2023), and EfficientNet (Tan & Le, 2019). These models focused on different aspects, including accuracy, efficiency, and scalability, while promoting valuable design principles. In recent years, inspired by ViTs, some CNNs (Liu et al., 2022; Woo et al., 2023; Ding et al., 2022; Liu et al., 2023) have incorporated large kernel convolutions to capture long-range dependencies, achieving performance competitive with ViT. At the same time, CNNs have been widely integrated into various ViTs and vision Mambas to enhance local modeling capabilities, creating a complementary synergy between the two approaches. These advancements have driven the diversification and convergence of model design in vision tasks.

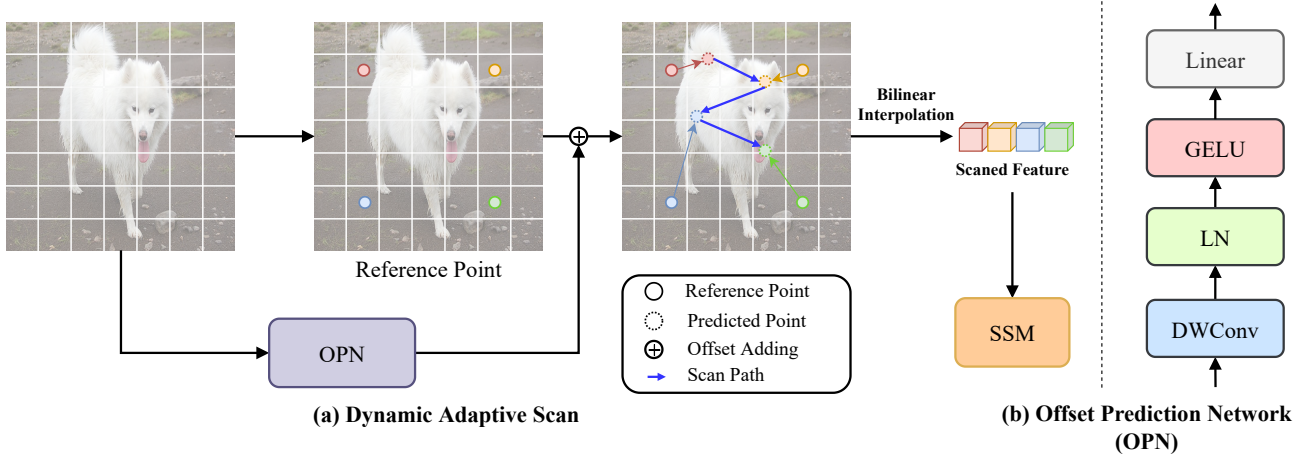


Figure 3. Illustration of the proposed Dynamic Adaptive Scan (DAS). For clarity, only four reference points are shown. **Left**: each initial reference point represents the original position of a patch, with its offsets learned by an Offset Prediction Network (OPN). Features of important regions are sampled based on the predicted 2D coordinates using bilinear interpolation. **Right** the detailed structure of the OPN is revealed. The query feature map is first transformed through depthwise convolution (Howard et al., 2017; Chollet, 2017) to integrate local information. Then, another linear layer, after layer normalization (Ba et al., 2016) and GELU (Hendrycks & Gimpel, 2016) activation, converts the feature map into offset values.

3. Methodology

3.1. Preliminaries

State Space Models (SSMs) (Gu et al., 2021; Gu & Dao, 2023) are a class of sequence modeling methods commonly used in deep learning, capable of representing dynamic systems through an intermediate latent state $h(t) \in \mathbb{R}^N$. Their core equations are as follows:

$$h'(t) = Ah(t) + Bx(t), \quad y(t) = Ch(t),$$

where the system matrices $A \in \mathbb{R}^{N \times N}$, $B \in \mathbb{R}^{N \times 1}$, and $C \in \mathbb{R}^{1 \times N}$ govern the dynamic evolution and output mapping.

To implement continuous-time models in practice, discretization techniques are required. The commonly used Zero-Order Hold (ZOH) method keeps the input constant within each time interval, transforming the continuous-time parameters (A, B) into their discrete forms as follows:

$$\bar{A} = e^{\Delta A}, \quad \bar{B} = (\Delta A)^{-1}(e^{\Delta A} - I)\Delta B,$$

where Δ represents the sampling time scale. The resulting discretized model can then be expressed as:

$$h_t = \bar{A}h_{t-1} + \bar{B}x_t, \quad y_t = Ch_t.$$

This method not only supports efficient parallel computation but also directly generates sequence outputs through convolution operations:

$$y = x * \bar{K}, \quad \bar{K} = (C\bar{B}, C\bar{A}\bar{B}, \dots, C\bar{A}^{L-1}\bar{B}),$$

where $\bar{K} \in \mathbb{R}^L$ is the SSM kernel, and $*$ denotes the convolution operation. This parallelization significantly enhances computational efficiency and scalability.

Although traditional SSMs (such as S4 (Gu et al., 2021)) achieve linear time complexity, their static parameterization limits their ability to capture the sequence context. To overcome this limitation, the Mamba (Gu & Dao, 2023) introduces a dynamic and input-dependent parameterization mechanism. Unlike traditional models that use constant transition parameters A, B , the Mamba model dynamically computes the parameters $B \in \mathbb{R}^{B \times L \times N}$, $C \in \mathbb{R}^{B \times L \times N}$, and $\Delta \in \mathbb{R}^{B \times L \times D}$ from the input sequence $x \in \mathbb{R}^{B \times L \times D}$. This allows for richer and more sequence-aware dynamic modeling.

In Mamba, continuous-time parameters are adaptively adjusted to input-dependent parameters through selective functions based on the input sequence x_t :

$$\Delta_t = s_\Delta(x_t), \quad B_t = s_B(x_t), \quad C_t = s_C(x_t),$$

and the input-dependent discrete parameters \bar{A}_t and \bar{B}_t can be calculated accordingly. The discrete state transition and observation equations are as follows:

$$h_t = \bar{A}_t h_{t-1} + \bar{B}_t x_t, \quad y_t = C_t h_t.$$

The dynamic parameterization of the Mamba model not only improves sequence modeling performance but also demonstrates strong competitiveness in language modeling and vision tasks. For instance: Vim (Zhu et al., 2024) combines bidirectional Mamba blocks to replace traditional Transformer blocks for visual modeling. VMamba (Liu et al.,

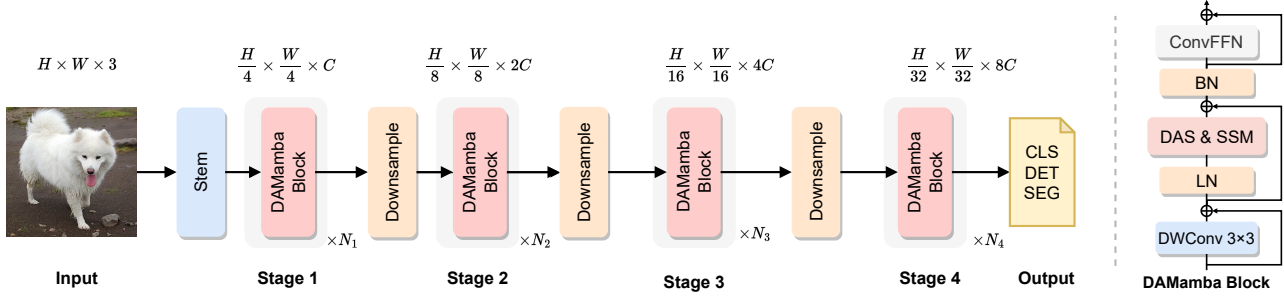


Figure 4. **Left:** The overall architecture of the proposed DAMamba, refer to Table 1 for configurations. **Right:** Details of an DAMamba Block.

2024) constructs a hierarchical structure by introducing 2D selective scanning, akin to the design of the Swin Transformer (Liu et al., 2021). These advancements expand the application potential of SSMs in foundational vision tasks, further driving the development of SSM models.

3.2. Dynamic Adaptive Scan

As shown in Figure 3, we propose Dynamic Adaptive Scan (DAS), which effectively models the relationships between image patches under the guidance of important regions in the feature map. These focused regions are determined by multiple sets of learnable sampling points, which are learned by an offset prediction network (OPN) from the input image feature map. After obtaining the two-dimensional coordinates predicted by the OPN, we use bilinear interpolation to sample features from the feature map, and then input the sampled features into the SSM for feature aggregation. Furthermore, the positions of DAS provide stronger relative positional biases to facilitate the learning of the SSM.

Specifically, we first input the feature map into an OPN to predict the two-dimensional coordinate offsets $\Delta p \in \mathbb{R}^{H \times W \times 2}$ of the interested patches relative to the original patches:

$$\Delta p = OPN([x_1, x_2, \dots, x_N]), \quad (1)$$

Then, these offsets are added to the positions of the original patches to determine the sampling locations of the interested patches:

$$p'[h, w, :] = p[h, w, :] + \Delta p[h, w, :], \quad (2)$$

where p' and p represent the sets of two-dimensional coordinates of the original patch and the interested patch on the feature map, respectively. p' and p take values between -1 and 1, (-1,-1) denotes the upper left corner, and (1,1) denotes the lower right corner. h and w denote the coordinates of the image patch in the height and width directions.

Next, we leverage position p' for feature sampling, which is performed through a bilinear interpolation function. By

establishing a relationship between the image patch features and the offsets, the proposed OPN can adaptively learn.

$$X'[h, w] = \phi(p'[h, w], X), \quad (3)$$

$$\phi(a, b) = \sum_{(r_x, r_y)} g(a_x, r_x, a_y, r_y) b[r_y, r_x, :], \quad (4)$$

$$g(c, d, e, f) = \max(0, 1 - |c - d|) \times \max(0, 1 - |e - f|), \quad (5)$$

where $g(c, d, e, f)$ represents the bi-linear sampling weight function, $a_x = p'[h, w, 0]$, $a_y = p'[h, w, 1]$, and (r_x, r_y) indexes all locations on $X \in \mathbb{R}^{H \times W \times C}$. g takes a nonzero value only at the four lattice points closest to the input location.

After obtaining the sampled feature vectors of interest, X' , we arrange them in the order of their original patches from top to bottom and left to right, and then input them into SSM for feature extraction.

3.3. Architecture Design of DAMamba

Table 1. Configurations for different DAMamba variants.

Models	Channels	Blocks
DAMamba-T	[80, 160, 320, 512]	[3, 4, 12, 5]
DAMamba-S	[96, 192, 384, 512]	[4, 8, 20, 6]
DAMamba-B	[112, 224, 448, 640]	[4, 8, 25, 8]

As shown in Figure 4, we propose a novel vision backbone named DAMamba base on DAS, and develop model variants at three scales: DAMamba-T, DAMamba-S and DAMamba-B. First, the input image $x \in \mathbb{R}^{H \times W \times 3}$ is processed through a stem module, consisting of 4 overlapping 3×3 convolutions, to generate a 2D feature map of size $\frac{H}{4} \times \frac{W}{4} \times C$. These features are then processed through four stages of continuous operations, forming a multi-scale hierarchical representation with resolutions of $\frac{H}{8} \times \frac{W}{8}$, $\frac{H}{16} \times \frac{W}{16}$, and $\frac{H}{32} \times \frac{W}{32}$, respectively. Each stage is composed of

multiple stacked DAMamba blocks, with resolution progressively downsampled by a factor of 2 and the feature dimension increased. Additionally, the DAMamba architecture integrates convolutional positional encoding (Chu et al., 2023; Islam et al., 2020; Li et al., 2021) and convolutional FFN (ConvFFN) (Wang et al., 2022), further enhancing the ability to extract local features. Throughout the architecture, DAMamba blocks are flexibly stacked across different stages to adapt to various downstream tasks. Finally, the model’s output undergoes batch normalization, global average pooling, and a linear classification head to produce the final image classification task feature representation. The configurations for different model scales are provided in Table 1.

4. Experiments

4.1. Image Classification on ImageNet-1K

Experimental settings: We conducted image classification experiments based on the ImageNet-1K dataset (Rusakovsky et al., 2015), which consists of 1,281,167 training images and 50,000 validation images spanning 1,000 categories. The implementation of our experimental methods relied on the PyTorch (Paszke et al., 2019) and Timm (Wightman et al., 2019) libraries. To ensure a fair comparison, we adopted the commonly used experimental settings from DeiT (Touvron et al., 2021). The optimizer used was AdamW (Loshchilov & Hutter, 2017), with a cosine decay learning rate schedule and linear warm-up over the first 20 epochs. The models were trained for 300 epochs on images with a resolution of 224^2 . For data augmentation and regularization, we employed techniques such as RandAugmentation (Cubuk et al., 2020), Repeated Augmentation (Hoffer et al., 2020), Mixup (Zhang et al., 2017), CutMix (Yun et al., 2019), Random Erasing (Zhong et al., 2020), weight decay, label smoothing (Szegedy et al., 2016), and stochastic depth (Huang et al., 2016). During testing, center cropping was applied to the validation images to generate input images with a resolution of 224^2 . The experiments were conducted on 16 RTX 3090 GPUs. Notably, exponential moving average (EMA) (Polyak & Juditsky, 1992) did not significantly improve the final model performance and was therefore not used in the experiments.

Results: As shown in Table 2, we compare the proposed DAMamba with several state-of-the-art models. The proposed DAMamba consistently outperforms ViT, CNN, and SSM models. Specifically, DAMamba-B achieves an accuracy of 85.2%, which is 1.3% higher than the current state-of-the-art SSM model (VMamba-B). Compared to the state-of-the-art CNN (ConvNeXt V2) and ViT (TransNext), the proposed DAMamba-T shows a significant improvement in accuracy. Even when the model is scaled to approximately 50M and 30M parameters, DAMamba achieves top-1

Table 2. Results of DAMamba and the current state-of-the-art backbones on ImageNet-1K. All the models are trained and tested at 224×224 resolution.

Model	Type	Params (M)	FLOPs (G)	Top-1 (%)
SLaK-T (Liu et al., 2023)	CNNs	30	5.0	82.5
ConvNeXt-T (Liu et al., 2022)	CNNs	29	4.5	82.1
InceptionNeXt-T (Yu et al., 2024)	CNNs	28	4.2	82.3
MambaOut-Tiny (Yu & Wang, 2024)	CNNs	27	4.5	82.7
UniRepLkNet-T (Ding et al., 2024)	CNNs	31	4.9	83.2
Swin-T (Liu et al., 2021)	ViTs	29	4.5	81.3
CSwin-T (Dong et al., 2022)	ViTs	23	4.3	82.7
Agent-Swin-T (Han et al., 2024)	ViTs	29	4.5	82.6
DAT-T (Xia et al., 2022)	ViTs	29	4.6	82.0
PVTv2-B2 (Wang et al., 2022)	ViTs	26	4.0	82.0
ClusterFormer-Tiny (Liang et al., 2023)	ViTs	28	-	81.5
Slide-PVT-S (Pan et al., 2023)	ViTs	23	4.0	81.7
NAT-T (Hassani et al., 2023)	ViTs	28	4.3	83.2
QFormer _s -T (Zhang et al., 2024)	ViTs	29	4.6	82.5
PartialFormer-B3 (Vo et al., 2024)	ViTs	36	3.4	83.0
StructViT-S-8-1 (Kim et al., 2024)	ViTs	24	5.4	83.3
Vim-S (Zhu et al., 2024)	SSMs	26	5.1	80.5
VMamba-T (Liu et al., 2024)	SSMs	22	5.6	82.6
LocalVMamba-T (Huang et al., 2024)	SSMs	26	5.7	82.7
DAMamba-T (ours)	SSMs	26	4.8	83.8
ConvNeXt-S (Liu et al., 2022)	CNNs	50	8.7	83.1
SLaK-S (Liu et al., 2023)	CNNs	55	9.8	83.8
InceptionNeXt-S (Yu et al., 2024)	CNNs	49	8.4	83.5
MambaOut-Small (Yu & Wang, 2024)	CNNs	48	9.0	84.1
UniRepLkNet-S (Ding et al., 2024)	CNNs	56	9.1	83.9
Swin-S (Liu et al., 2021)	ViTs	50	8.7	83.0
Agent-Swin-S (Han et al., 2024)	ViTs	50	8.7	83.7
NAT-S (Hassani et al., 2023)	ViTs	51	7.8	83.7
PVTv2-B4 (Wang et al., 2022)	ViTs	63	10.1	83.6
DAT-S (Xia et al., 2022)	ViTs	50	9.0	83.7
ClusterFormer-Small (Liang et al., 2023)	ViTs	49	-	83.4
QFormer _s -S (Zhang et al., 2024)	ViTs	51	8.9	84.0
BiFormer-B (Zhu et al., 2023)	ViTs	57	9.8	84.3
PartialFormer-B4 (Vo et al., 2024)	ViTs	64	6.8	83.9
StructViT-B-8-1 (Kim et al., 2024)	ViTs	52	12.0	84.3
TransNeXt-Small (Shi, 2024)	ViTs	50	10.3	84.7
VMamba-S (Liu et al., 2024)	SSMs	44	11.2	83.6
LocalVMamba-S (Huang et al., 2024)	SSMs	50	11.4	83.7
DAMamba-S (ours)	SSMs	45	10.3	84.8
ConvNeXt-B (Liu et al., 2022)	CNNs	89	15.4	83.8
SLaK-B (Liu et al., 2023)	CNNs	95	17.1	84.0
InceptionNeXt-B (Yu et al., 2024)	CNNs	87	14.9	84.0
MambaOut-Base (Yu & Wang, 2024)	CNNs	85	15.8	84.2
Swin-B (Liu et al., 2021)	ViTs	88	15.4	83.5
CSwin-B (Dong et al., 2022)	ViTs	78	15.0	84.2
Agent-Swin-B (Han et al., 2024)	ViTs	88	15.4	84.0
NAT-B (Hassani et al., 2023)	ViTs	90	13.7	84.3
PVTv2-B5 (Wang et al., 2022)	ViTs	82	11.8	83.8
FLatten-Swin-B (Han et al., 2023)	ViTs	89	15.4	83.8
DAT-B (Xia et al., 2022)	ViTs	88	15.8	84.0
QFormer _s -B (Zhang et al., 2024)	ViTs	90	15.7	84.1
TransNeXt-Base (Shi, 2024)	ViTs	90	18.4	84.8
VMamba-B (Liu et al., 2024)	SSMs	75	18.0	83.9
DAMamba-B (ours)	SSMs	86	16.3	85.2

accuracies of 83.8% and 84.8%, maintaining its excellent performance.

4.2. Object Detection and Instance Segmentation on COCO2017

Experimental settings: We conducted object detection and instance segmentation experiments on the COCO 2017 dataset. The COCO 2017 dataset (Lin et al., 2014) consists of approximately 118K training images and 5K validation images and serves as a commonly used benchmark for object detection and instance segmentation tasks. To evaluate the performance of the proposed model on downstream vision tasks, we selected DAMamba as the backbone network and

embedded it into a detector to extract object and instance features from images. DAMamba was integrated into the classic Mask R-CNN (He et al., 2017) detector and initialized with weights pre-trained on the ImageNet-1K dataset for 300 epochs. For the object detection and instance segmentation tasks, we trained the model for 12 epochs ($1\times$) and 36 epochs ($3\times$). All experiments were conducted using the MMDetection (Chen et al., 2019) framework.

Results: The object detection and instance segmentation results of DAMamba on the COCO2017 dataset are shown in Table 3. In terms of bounding box and mask average precision (AP^b and AP^m), DAMamba demonstrates outstanding performance. Using a ($1\times$) fine-tuning schedule, DAMamba-T/S/B achieves object detection mAPs of 48.5/49.8/50.6, outperforming VMamba-T/S/B by 1.2/1.1/1.4 mAP, Swin-T/S/B by 5.8/5.0/3.7 mAP, and ConvNeXt-T/S/B by 4.3/4.4/3.6 mAP. Under the same configuration, the instance segmentation mAP of DAMamba-T/S/B also significantly outperforms VMamba-T/S/B, Swin-T/S/B and ConvNeXt-T/S/B. When using a $3\times$ training configuration, DAMamba still maintains large performance improvements. These results indicate that DAMamba has the potential to achieve state-of-the-art performance in dense prediction downstream tasks.

4.3. Semantic Segmentation on ADE20K

Experimental settings: We conducted semantic segmentation experiments using the ADE20K dataset and performed a comparative analysis of DAMamba and other models within the UperNet (Xiao et al., 2018) framework. In the UperNet framework, the backbone network was initialized with weights pre-trained on the ImageNet-1K dataset, while the remaining parts were randomly initialized. The model optimization employed the AdamW optimizer with a batch size of 16. To ensure a fair comparison, all models were trained for 160k iterations within the UperNet framework. All experiments were conducted using the MMSegmentation (Contributors, 2020) framework.

Results: Table 4 presents the semantic segmentation results of DAMamba under the UperNet (Xiao et al., 2018) framework. The experiments show that DAMamba-T/S/B achieves mIoU scores of 50.3%, 51.2%, and 51.9%, respectively, significantly outperforming other types of models. The performance improvement of our DAMamba is also evident when using multi-scale tests. These results further validate the exceptional generalization capability of DAMamba in downstream tasks.

4.4. Ablation Study

To validate the effectiveness of our method, we conducted image classification ablation experiments on ImageNet-1k using DAMamba-T in Table 5. Compared to the baseline

Table 3. Comparison of object detection and instance segmentation performance on COCO with Mask R-CNN detector. FLOPs are calculated with input resolution of 1280×800 .

Mask R-CNN $1\times$ schedule								
Backbone	AP^b	AP^b_{50}	AP^b_{75}	AP^m	AP^m_{50}	AP^m_{75}	#Param.	FLOPs
Swin-T	42.7	65.2	46.8	39.3	62.2	42.2	48M	267G
DAT-T	44.4	67.6	48.5	42.4	66.1	45.5	48M	272G
CSWin-T	46.7	68.6	51.3	42.2	65.6	45.4	42M	279G
ConvNeXt-T	44.2	66.6	48.3	40.1	63.3	42.8	48M	262G
PVTv2-B2	45.3	66.1	49.6	41.2	64.2	44.4	45M	309G
QFormer _h -T	45.9	68.5	50.3	41.5	65.2	44.6	49M	-
PartialFormer-B3	45.0	-	-	40.9	-	-	54M	248G
BiFormer-S	47.8	69.8	52.3	43.2	66.8	46.5	-	-
MambaOut-T	45.1	67.3	49.6	41.0	64.1	44.1	43M	262G
VMamba-T	47.3	69.3	52.0	42.7	66.4	45.9	50M	271G
LocalVMamba-T	46.7	68.7	50.8	42.2	65.7	45.5	45M	291G
DAMamba-T	48.5	70.3	53.3	43.4	67.2	46.7	45M	284G
Swin-S	44.8	68.6	49.4	40.9	65.3	44.2	69M	354G
Agent-Swin-S	47.2	69.6	52.3	42.7	66.6	45.8	-	364G
DAT-S	47.1	69.9	51.5	42.5	66.7	45.4	69M	378G
CSWin-S	47.9	70.1	52.6	43.2	67.1	46.2	54M	342G
ConvNeXt-S	45.4	67.9	50.0	41.8	65.2	45.1	70M	348G
PVTv2-B3	47.0	68.1	51.7	42.5	65.2	45.7	63M	397G
BiFormer-B	48.6	70.5	53.8	43.7	67.6	47.1	-	-
MambaOut-S	47.4	69.1	52.4	42.7	66.1	46.2	65M	354G
VMamba-S	48.7	70.0	53.4	43.7	67.3	47.0	70M	349G
LocalVMamba-S	48.4	69.9	52.7	43.2	66.7	46.5	69M	414G
DAMamba-S	49.8	71.2	54.7	44.5	68.4	48.2	65M	395G
Swin-B	46.9	69.2	51.6	42.3	66.0	45.5	88M	496G
CSwin-B	48.7	70.4	53.9	43.9	67.8	47.3	88M	496G
ConvNeXt-B	47.0	69.4	51.7	42.7	66.3	46.0	107M	486G
PVTv2-B5	47.4	68.6	51.9	42.5	65.7	46.0	102M	557G
ViT-Adapter-B	47.0	68.2	51.4	41.8	65.1	44.9	102M	557G
MambaOut-B	47.4	69.3	52.2	43.0	66.4	46.3	100M	495G
VMamba-B	49.2	71.4	54.0	44.1	68.3	47.7	108M	485G
DAMamba-B	50.6	71.9	55.5	44.9	68.9	48.7	105M	520G
Mask R-CNN $3\times$ MS schedule								
Backbone	AP^b	AP^b_{50}	AP^b_{75}	AP^m	AP^m_{50}	AP^m_{75}	#Param.	FLOPs
Swin-T	46.0	68.1	50.3	41.6	65.1	44.9	48M	267G
PVTv2-B2	47.8	69.7	52.6	43.1	66.8	46.7	45M	309G
ConvNeXt-T	46.2	67.9	50.8	41.7	65.0	44.9	48M	262G
NAT-T	47.7	69.0	52.6	42.6	66.1	45.9	48M	258G
QFormer _h -T	47.5	69.6	52.1	42.7	66.4	46.1	49M	-
VMamba-T	48.8	70.4	53.5	43.7	67.4	47.0	50M	271G
LocalVMamba-T	48.7	70.1	53.0	43.4	67.0	46.4	45M	291G
DAMamba-T	50.4	71.4	55.5	44.8	68.6	48.6	45M	284G
Swin-S	48.2	69.8	52.8	43.2	67.0	46.1	69M	354G
PVTv2-B3	48.4	69.8	53.3	43.2	66.9	46.7	65M	397G
ConvNeXt-S	47.9	70.0	52.7	42.9	66.9	46.2	70M	348G
NAT-S	48.4	69.8	53.2	43.2	66.9	46.5	70M	330G
QFormer _h -S	49.5	71.2	54.2	44.2	68.3	47.6	70M	-G
VMamba-S	49.9	70.9	54.7	44.2	68.2	47.7	70M	349G
LocalVMamba-S	49.9	70.5	54.4	44.1	67.8	47.4	69M	414G
DAMamba-S	51.2	72.1	56.1	45.1	69.2	49.1	65M	395G
ConvNeXt-B	48.5	70.1	53.3	43.5	67.1	46.7	108M	486G
Swin-B	48.6	70.0	53.4	43.3	67.1	46.7	107M	496G
PVTv2-B5	48.4	69.2	52.9	42.9	66.6	46.2	102M	557G
DAMamba-B	51.4	72.3	56.4	45.3	69.5	48.9	105M	520G

model with Sweeping Scan, our proposed Dynamic Adaptive Scan (DAS) improves the top-1 accuracy by 0.4% while consuming only a small amount of additional FLOPs and parameter overhead. Furthermore, for the vision SSMs, which excels at global modeling, we observe that using convolutional positional encoding (Convpos) (Chu et al., 2023; Islam et al., 2020; Li et al., 2021) and ConvFFN (Wang et al., 2022) for local modeling can improve accuracy by

Table 4. Comparison of semantic segmentation on ADE20K with UPerNet segmentor. FLOPs are calculated with input resolution of 512×2048 . ‘SS’ and ‘MS’ represent single-scale and multi-scale testing, respectively.

Method	mIoU (SS)	mIoU (MS)	#Param.	FLOPs
UniRepLKNet-T	48.6	49.1	61M	946G
ConvNeXt-T	46.0	46.7	60M	939G
Swin-T	44.4	45.8	60M	945G
Agent-Swin-T	46.7	-	61M	954G
NAT-T	47.1	48.4	58M	934G
QFormer _i -T	46.9	48.1	61M	-
PartialFormer-B3	47.0	-	65M	923G
BiFormer-S	49.8	50.8	-	-
MambaOut-T	47.4	48.6	54M	938G
VMamba-T	48.0	48.8	62M	949G
LocalVMamba-T	47.9	49.1	57M	970G
DAMamba-T	50.3	51.2	55M	937G
UniRepLKNet-S	50.5	51.0	86M	1036G
Swin-S	47.6	49.5	81M	1039G
Agent-Swin-S	48.1	-	81M	1043G
ConvNeXt-S	48.7	49.6	82M	1027G
NAT-S	48.0	49.5	82M	1010G
QFormer _i -S	48.9	50.3	82M	-
PartialFormer-B3	48.3	-	95M	1005G
BiFormer-B	51.0	51.7	-	-
MambaOut-S	49.5	50.6	76M	1032G
VMamba-S	50.6	51.2	82M	1028G
LocalVMamba-S	50.0	51.0	81M	1095G
DAMamba-S	51.2	52.0	75M	1050G
Swin-B	48.1	49.7	121M	1188G
Agent-Swin-B	48.7	-	121M	1196G
ConvNeXt-B	49.1	49.9	122M	1170G
NAT-B	48.5	49.7	123M	1137G
QFormer _i -B	49.5	50.6	123M	-
MambaOut-B	49.6	51.0	112M	1178G
VMamba-B	51.0	51.6	122M	1170G
DAMamba-B	51.9	52.3	117M	1178G

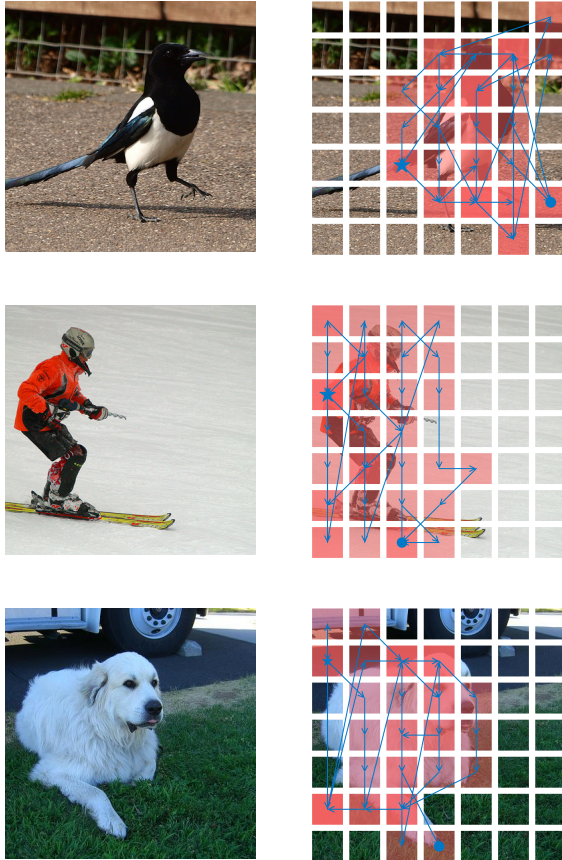
Table 5. Ablation studies on DAMamba-T for module designs.

Module design	#Param. (M)	FLOPs (G)	Top-1 acc (%)
Baseline	24.7M	4.66G	80.8
+ DAScan	25.1M	4.73G	81.2
+ Convpos	25.2M	4.75G	81.4
+ ConvFFN	25.5M	4.82G	81.8

0.2% and 0.4%, respectively.

4.5. Visualization

As shown in Figure 5, we visualize the scanning results of DAMamba on ImageNet-1K images to verify the effectiveness of the proposed dynamic adaptive scanning method. For ease of visualization, we selected the final stage with fewer patches and removed prediction points outside the region of interest. For 2D positions of floating-point type, we visualize them by mapping each position to the nearest patch. We present three examples from the ImageNet-1K dataset. We observe that the proposed dynamic adaptive scanning primarily focuses on target objects, adapting to the input image by dynamically focusing on the foreground regions of interest. Additionally, the scanning areas can be adaptively adjusted.



(a) Input image.

(b) Scan Path.

Figure 5. Visualization of the Dynamic Adaptive Scan, where the blue pentagram represents the start of the scan and the blue circle represents the end of the scan.

5. Conclusion

In this paper, we have proposed a novel vision state space model, termed DAMamba. DAMamba significantly enhances the flexibility of modeling in vision SSMs and improves the ability to capture complex image structures, while maintaining both local and global contextual understanding. Specifically, a Dynamic Adaptive Scan mechanism is proposed to adaptively allocate scanning order and regions based on the input image. Extensive experiments on various datasets and popular vision tasks demonstrate that the proposed DAMamba significantly and consistently outperforms the state-of-the-art vision SSMs as well as popular ViT and CNN architectures, establishing new benchmarks for image classification, object detection, instance segmentation, and semantic segmentation. Our findings underscore the importance of the scanning mechanism in vision SSMs and highlight the tremendous potential of SSMs as vision backbone.

References

- Ba, J., Kiros, J., and Hinton, G. Layer normalization, Jul 2016.
- Chen, K., Wang, J., Pang, J., Cao, Y., Xiong, Y., Li, X., Sun, S., Feng, W., Liu, Z., Xu, J., et al. Mmdetection: Open mmlab detection toolbox and benchmark. *arXiv preprint arXiv:1906.07155*, 2019.
- Chollet, F. Xception: Deep learning with depthwise separable convolutions. In *CVPR*, pp. 1251–1258, 2017.
- Chu, X., Tian, Z., Zhang, B., Wang, X., and Shen, C. Conditional positional encodings for vision transformers. In *ICLR*, 2023. URL <https://openreview.net/forum?id=3KWnuT-R1bh>.
- Contributors, M. Mmsegmentation: Openmmlab semantic segmentation toolbox and benchmark, 2020.
- Cubuk, E. D., Zoph, B., Shlens, J., and Le, Q. V. Randaugment: Practical automated data augmentation with a reduced search space. In *CVPRW*, pp. 702–703, 2020.
- Ding, X., Zhang, X., Han, J., and Ding, G. Scaling up your kernels to 31x31: Revisiting large kernel design in cnns. In *CVPR*, pp. 11963–11975, 2022.
- Ding, X., Zhang, Y., Ge, Y., Zhao, S., Song, L., Yue, X., and Shan, Y. Unireplknet: A universal perception large-kernel convnet for audio video point cloud time-series and image recognition. In *CVPR*, pp. 5513–5524, 2024.
- Dong, X., Bao, J., Chen, D., Zhang, W., Yu, N., Yuan, L., Chen, D., and Guo, B. Cswin transformer: A general vision transformer backbone with cross-shaped windows. In *CVPR*, pp. 12124–12134, 2022.
- Dosovitskiy, A., Beyer, L., Kolesnikov, A., Weissenborn, D., Zhai, X., Unterthiner, T., Dehghani, M., Minderer, M., Heigold, G., Gelly, S., et al. An image is worth 16x16 words: Transformers for image recognition at scale. In *ICLR*, 2021.
- Gu, A. and Dao, T. Mamba: Linear-time sequence modeling with selective state spaces. *arXiv preprint arXiv:2312.00752*, 2023.
- Gu, A., Goel, K., and Ré, C. Efficiently modeling long sequences with structured state spaces. *arXiv preprint arXiv:2111.00396*, 2021.
- Han, D., Pan, X., Han, Y., Song, S., and Huang, G. Flatten transformer: Vision transformer using focused linear attention. In *ICCV*, pp. 5961–5971, 2023.
- Han, D., Ye, T., Han, Y., Xia, Z., Pan, S., Wan, P., Song, S., and Huang, G. Agent attention: On the integration of softmax and linear attention. In *ECCV*, pp. 124–140. Springer, 2024.
- Hassani, A., Walton, S., Li, J., Li, S., and Shi, H. Neighborhood attention transformer. In *CVPR*, pp. 6185–6194, 2023.
- He, K., Zhang, X., Ren, S., and Sun, J. Deep residual learning for image recognition. In *CVPR*, pp. 770–778, 2016.
- He, K., Gkioxari, G., Dollár, P., and Girshick, R. Mask r-cnn. In *ICCV*, pp. 2961–2969, 2017.
- Hendrycks, D. and Gimpel, K. Gaussian error linear units (gelus). *arXiv preprint arXiv:1606.08415*, 2016.
- Hinton, G., Vinyals, O., and Dean, J. Distilling the knowledge in a neural network. *arXiv preprint arXiv:1503.02531*, 2015.
- Hoffer, E., Ben-Nun, T., Hubara, I., Giladi, N., Hoefler, T., and Soudry, D. Augment your batch: Improving generalization through instance repetition. In *CVPR*, pp. 8129–8138, 2020.
- Howard, A. G., Zhu, M., Chen, B., Kalenichenko, D., Wang, W., Weyand, T., Andreetto, M., and Adam, H. Mobilenets: Efficient convolutional neural networks for mobile vision applications. *arXiv preprint arXiv:1704.04861*, 2017.
- Huang, G., Sun, Y., Liu, Z., Sedra, D., and Weinberger, K. Q. Deep networks with stochastic depth. In *ECCV*, pp. 646–661. Springer, 2016.
- Huang, G., Liu, Z., Van Der Maaten, L., and Weinberger, K. Q. Densely connected convolutional networks. In *CVPR*, pp. 4700–4708, 2017.
- Huang, T., Pei, X., You, S., Wang, F., Qian, C., and Xu, C. Localmamba: Visual state space model with windowed selective scan. *arXiv preprint arXiv:2403.09338*, 2024.
- Islam, A., Jia, S., and Bruce, N. D. B. How much position information do convolutional neural networks encode. *arXiv preprint arXiv:2001.08248*, 2020.
- Jiao, J., Tang, Y.-M., Lin, K.-Y., Gao, Y., Ma, J., Wang, Y., and Zheng, W.-S. Dilateformer: Multi-scale dilated transformer for visual recognition. *TMM*, 2023.
- Kim, M., Seo, P. H., Schmid, C., and Cho, M. Learning correlation structures for vision transformers. In *CVPR*, pp. 18941–18951, 2024.
- Krizhevsky, A., Sutskever, I., and Hinton, G. E. Imagenet classification with deep convolutional neural networks. In *NeurIPS*, pp. 1097–1105, 2012.

- LeCun, Y., Bottou, L., Bengio, Y., and Haffner, P. Gradient-based learning applied to document recognition. *Proceedings of the IEEE*, 86(11):2278–2324, 1998.
- Li, Y., Zhang, K., Cao, J., Timofte, R., and Gool, L. V. Localvit: Bringing locality to vision transformers. *arXiv preprint arXiv:2104.05707*, 2021.
- Liang, J. C., Cui, Y., Wang, Q., Geng, T., Wang, W., and Liu, D. Clusterformer: Clustering as a universal visual learner. *NeurIPS*, 2023.
- Lin, T.-Y., Maire, M., Belongie, S., Hays, J., Perona, P., Ramanan, D., Dollár, P., and Zitnick, C. L. Microsoft coco: Common objects in context. In *ECCV*, pp. 740–755. Springer, 2014.
- Liu, S., Chen, T., Chen, X., Chen, X., Xiao, Q., Wu, B., Kärkkäinen, T., Pechenizkiy, M., Mocanu, D. C., and Wang, Z. More convnets in the 2020s: Scaling up kernels beyond 51x51 using sparsity. In *ICLR*, 2023.
- Liu, Y., Tian, Y., Zhao, Y., Yu, H., Xie, L., Wang, Y., Ye, Q., and Liu, Y. Vmamba: Visual state space model. In *NeurIPS*, 2024.
- Liu, Z., Lin, Y., Cao, Y., Hu, H., Wei, Y., Zhang, Z., Lin, S., and Guo, B. Swin transformer: Hierarchical vision transformer using shifted windows. In *ICCV*, pp. 10012–10022, 2021.
- Liu, Z., Mao, H., Wu, C.-Y., Feichtenhofer, C., Darrell, T., and Xie, S. A convnet for the 2020s. In *CVPR*, pp. 11976–11986, 2022.
- Loshchilov, I. and Hutter, F. Decoupled weight decay regularization. *arXiv preprint arXiv:1711.05101*, 2017.
- Pan, X., Ye, T., Xia, Z., Song, S., and Huang, G. Slide-transformer: Hierarchical vision transformer with local self-attention. In *CVPR*, pp. 2082–2091, 2023.
- Paszke, A., Gross, S., Massa, F., Lerer, A., Bradbury, J., Chanan, G., Killeen, T., Lin, Z., Gimelshein, N., Antiga, L., et al. Pytorch: An imperative style, high-performance deep learning library. *NeurIPS*, 32, 2019.
- Polyak, B. T. and Juditsky, A. B. Acceleration of stochastic approximation by averaging. *SIAM Journal on Control and Optimization*, 30(4):838–855, 1992.
- Russakovsky, O., Deng, J., Su, H., Krause, J., Satheesh, S., Ma, S., Huang, Z., Karpathy, A., Khosla, A., Bernstein, M., et al. Imagenet large scale visual recognition challenge. *IJCV*, 115:211–252, 2015.
- Shi, D. Transnext: Robust foveal visual perception for vision transformers. In *CVPR*, pp. 17773–17783, 2024.
- Simonyan, K. and Zisserman, A. Very deep convolutional networks for large-scale image recognition. *arXiv preprint arXiv:1409.1556*, 2014.
- Szegedy, C., Liu, W., Jia, Y., Sermanet, P., Reed, S., Anguelov, D., Erhan, D., Vanhoucke, V., and Rabinovich, A. Going deeper with convolutions. In *CVPR*, pp. 1–9, 2015.
- Szegedy, C., Vanhoucke, V., Ioffe, S., Shlens, J., and Wojna, Z. Rethinking the inception architecture for computer vision. In *CVPR*, pp. 2818–2826, 2016.
- Tan, M. and Le, Q. Efficientnet: Rethinking model scaling for convolutional neural networks. In *ICML*, pp. 6105–6114. PMLR, 2019.
- Touvron, H., Cord, M., Douze, M., Massa, F., Sablayrolles, A., and Jégou, H. Training data-efficient image transformers & distillation through attention. In *ICML*, pp. 10347–10357. PMLR, 2021.
- Vaswani, A., Shazeer, N., Parmar, N., Uszkoreit, J., Jones, L., Gomez, A. N., Kaiser, Ł., and Polosukhin, I. Attention is all you need. *NeurIPS*, 30, 2017.
- Vo, X.-T., Nguyen, D.-L., Priadana, A., and Jo, K.-H. Efficient vision transformers with partial attention. In *ECCV*, pp. 298–317. Springer, 2024.
- Wang, W., Xie, E., Li, X., Fan, D.-P., Song, K., Liang, D., Lu, T., Luo, P., and Shao, L. Pyramid vision transformer: A versatile backbone for dense prediction without convolutions. In *ICCV*, pp. 568–578, 2021.
- Wang, W., Xie, E., Li, X., Fan, D.-P., Song, K., Liang, D., Lu, T., Luo, P., and Shao, L. Pvt v2: Improved baselines with pyramid vision transformer. *CVM*, 8(3):415–424, 2022.
- Wang, W., Dai, J., Chen, Z., Huang, Z., Li, Z., Zhu, X., Hu, X., Lu, T., Lu, L., Li, H., et al. Internimage: Exploring large-scale vision foundation models with deformable convolutions. In *CVPR*, pp. 14408–14419, 2023.
- Wightman, R. et al. Pytorch image models, 2019.
- Woo, S., Debnath, S., Hu, R., Chen, X., Liu, Z., Kweon, I. S., and Xie, S. Convnext v2: Co-designing and scaling convnets with masked autoencoders. In *CVPR*, pp. 16133–16142, 2023.
- Xia, Z., Pan, X., Song, S., Li, L. E., and Huang, G. Vision transformer with deformable attention. In *CVPR*, pp. 4794–4803, 2022.
- Xiao, T., Liu, Y., Zhou, B., Jiang, Y., and Sun, J. Unified perceptual parsing for scene understanding. In *ECCV*, pp. 418–434, 2018.

- Yang, C., Chen, Z., Espinosa, M., Ericsson, L., Wang, Z., Liu, J., and Crowley, E. J. Plainmamba: Improving non-hierarchical mamba in visual recognition. *arXiv preprint arXiv:2403.17695*, 2024.
- Yu, W. and Wang, X. Mambaout: Do we really need mamba for vision? *arXiv preprint arXiv:2405.07992*, 2024.
- Yu, W., Zhou, P., Yan, S., and Wang, X. Inceptionnext: When inception meets convnext. In *CVPR*, pp. 5672–5683, 2024.
- Yun, S., Han, D., Oh, S. J., Chun, S., Choe, J., and Yoo, Y. Cutmix: Regularization strategy to train strong classifiers with localizable features. In *ICCV*, pp. 6023–6032, 2019.
- Zhang, H., Cisse, M., Dauphin, Y. N., and Lopez-Paz, D. mixup: Beyond empirical risk minimization. *arXiv preprint arXiv:1710.09412*, 2017.
- Zhang, L., Li, X., Arnab, A., Yang, K., Tong, Y., and Torr, P. H. Dual graph convolutional network for semantic segmentation. *arXiv preprint arXiv:1909.06121*, 2019.
- Zhang, Q., Zhang, J., Xu, Y., and Tao, D. Vision transformer with quadrangle attention. *TPAMI*, 2024.
- Zhong, Z., Zheng, L., Kang, G., Li, S., and Yang, Y. Random erasing data augmentation. In *AAAI*, pp. 13001–13008, 2020.
- Zhu, L., Wang, X., Ke, Z., Zhang, W., and Lau, R. W. Bi-former: Vision transformer with bi-level routing attention. In *CVPR*, pp. 10323–10333, 2023.
- Zhu, L., Liao, B., Zhang, Q., Wang, X., Liu, W., and Wang, X. Vision mamba: Efficient visual representation learning with bidirectional state space model. In *ICML*, 2024.